Title

An assessment of controlled source EM for monitoring subsurface CO2 injection at the wyoming carbonSAFE geologic carbon storage site

Authors

Alumbaugh, David
Um, Evan Schankee
Moe, Giacobe
et al.

Publication Date

2024-09-01

DOI

10.1016/j.ijggc.2024.104229

Title: An Assessment of Controlled Source EM for Monitoring Subsurface CO_2 Injection at the Wyoming CarbonSAFE Geologic Carbon Storage Site

List of authors:

*David Alumbaugh, Earth and Environmental Sciences, Lawrence Berkeley National Laboratory, One Cyclotron Road, Mail Stop 74R316C, Berkeley, California, 94720, dlalumbaugh@lbl.gov

Evan Schankee Um, Earth and Environmental Sciences, Lawrence Berkeley National Laboratory, Berkeley, California, esum@lbl.gov

Giacobe Moe, Zonge International, giacobe.moe@zonge.com

Wanjie Feng, Zonge International, wanjie.feng@zonge.com

*Corresponding Author

Keywords:

Carbon Storage

Carbon Sequestration

Subsurface Monitoring

Abstract

We evaluate if electromagnetic (EM) geophysical methods for monitoring geologic carbon storage (GCS) efforts at the Wyoming CarbonSAFE project adjacent to the Dry Fork Station power plant near Gillette, Wyoming. This first involved acquiring both electric and magnetic fields at eleven different locations ranging in distance from immediately adjacent to 4 km from the plant. Passive EM measurements were made to provide spectral EM noise measurements generated by electricity production at the plant and to determine if useful magnetotelluric (MT) data can be successfully collected in the region. The processed data indicate that useful MT data can be collected as long as the site is located more than 2km away from the power plant as well as active roads and rail lines. Controlled source EM data were collected using three different source configurations, two of which connected to steel casings used to complete the injection wells. Comparing the EM noise measurements to the CSEM data show measurable electric and magnetic field signals at all sites. Next a series of three-dimensional (3D) numerical models were built that simulate resistivity changes caused by the proposed CO_2 injection at depths ranging from 2.4 to 3.0km. These models were used to simulate various EM measurement configurations. The modeling shows that casing-source CSEM monitoring can provide sensitivity to the injected CO_2 if source electrodes are connected to the bottom of one or both of the injection wells.

Introduction

As part of a coordinated effort to reduce green-house gas emissions, and specifically CO_2 into the atmosphere, the International Energy Agency's Net-Zero Emissions by 2050 Scenario, which results from techno-economic modeling of the portion of the global economy that emits greenhouse gasses, has 7.6 gigatonnes (Gt) of CO2 captured in 2050 (IEA, 2021) with 95% of the captured CO_2 being sequestered in supercritical form ($scCO_2$) in underground formations. As a significant contributor of worldwide CO_2, the US has agreed to pursue and promote carbon capture, utilization and storage (CCUS) projects as major component of its effort of zero net emissions by 2050. Different scenarios published by Larson et al. (2021) and Suter et al. (2022) suggest that this will involve the US capturing and sequestering 0.4 to 1.7 Gt in 2050. Alumbaugh et al. (2024) suggest a number of scenarios of how the US CCUS industry will grow between now and 2050 to meet these goals.

Since 2016, the US Department of Energy (DOE) has been investing in the development of a US CCUS industry through its Carbon Storage Assurance Facility Enterprise (CarbonSAFE) Initiative (see https://netl.doe.gov/carbon-management/carbon-storage/carbonsafe#:~:text=The%20Carbon%20Storage%20Assurance%20Facility,and%20Storage%20(CCS)%20deployment for more information). A requirement of receiving CarbonSAFE funding is that proposed project has the potential to capture and store 50 metric mega-tonnes (Mt) within a 30 year lifetime. CarbonSAFE projects are chosen / awarded through a proposal submission in response to DOE funding announcements, with the participants proposing to satisfy one of four stages of CCUS development:

- Phase I – Integrated pre-feasibility projects which involve an economic feasibility study as well as the collection and analysis of available region data sets;

- Phase II – Storage complex feasibility projects which involve the drilling of a stratigraphic well and the acquisition of geologic and geophysical data as well as performing well tests;
- Phase III – Site characterization and permitting which focusses on acquiring all necessary data to write and submit an Environmental Protection Agency (EPA) Class VI permit application necessary to construct and operate a CO_2 injection well for sequestration purposes, and;
- Phase IV – Construction which helps with construction costs once the Class VI permit is approved by the EPA.

One component that must be included in a successful Class VI permit application is a subsurface monitoring plan, where the goal of the monitoring is to verify conformance that the injected scCO_2 is behaving as expected, and that there is no leakage of CO_2 or brine into potable groundwater supplies above the saline reservoirs. Alumbaugh et al. (2024) analyzed approximately 60 EPA Class VI permit applications that had been filed by the end of October 2023 and found that the dominant geophysical monitoring method proposed is time lapse 2D or 3D seismic and/or vertical seismic profile (VSP) imaging surveys repeated every two to five years. Although seismic imaging generally provides superior resolution at reservoir depths compared to methods like electromagnetic (EM) and gravity, there are certain geological conditions where seismic properties might not show significant changes with CO_2 injection. For example, older sandstone reservoir units can be very stiff, making them less responsive to changes in CO_2 saturation in terms of altering the rock's seismic velocity. Secondly, highly heterogeneous sandstone reservoirs often contain thin, high-permeability layers and this coupled with the buoyancy of the CO_2 can result in thin plumes which are difficult to detect and monitor with seismic methods. In these situations, EM methods can be particularly useful for monitoring these types of plumes as supercritical CO_2 has much higher resistivity than the native fluids filling the pore space in saline reservoirs. As a result, electrical resistivity of porous sedimentary rocks will experience larger changes when CO_2 replaces brine (e.g., Wilt and Alumbaugh, 1998), compared to changes in seismic velocity or density.

Seismic and electromagnetic (EM) methods can complement each other for more reliable CO2 plume monitoring. For example, p-wave velocity is generally more sensitive to injected CO_2 at low saturations (up to 20%) but shows little changes at high saturation (Vasco et al., 2014). Thus, seismic methods are well-suited for delineating the boundaries of CO2 plumes. In contrast, the electrical resistivity doesn't change much at low CO_2 saturation but changes more rapidly at higher saturations, making EM methods ideal for characterizing the saturation across the plume. Additionally, integrating multi-physics data from various methods, including seismic and EM, can further improve resolution and reduce uncertainty in geophysical imaging (e.g., Gallardo and Meju, 2003; Colombo and Rovetta, 2018; Giraud et al., 2017; Um et al., 2022).

For the reasons mentioned above, we have been investigating EM techniques as a complimentary method for subsurface seismic monitoring, and specifically the idea of electrically energizing the steel well casings used to complete injection and monitoring wells as part of the EM source. Using the steel casings as part of the source enhances the energy being transmitted into the reservoir thus providing better sensitivity to the electrically resistive CO_2 (Masala et al., 2014; MacLennan, 2022). However, because many geological carbon storage sites are located near power plants or other industrial facilities, there are questions around whether or not the electromagnetic signals generated by these facilities will overwhelm the signals that we are trying to measure from the reservoir. To address this, scientists from Lawrence Berkeley National Laboratory (LBNL) and the University of Wyoming, who are leading the Wyoming CarbonSAFE project, a geological carbon storage research initiative adjacent to the Dry Fork Power Station near Gillette, WY, conducted an EM field measurement and modeling study.

Below we provide a brief overview of the Dry Fork Station power plant and the geology associated with the Wyoming CarbonSAFE site. This will be followed by a description and analysis of the field measurements that were made to determine both naturally occurring and power-station generated noise at the site. In the last section we provide results of a modeling study that investigates the sensitivity of the energized-casing source configuration for monitoring the sequestered CO_2.

Overview of the Wyoming CarbonSAFE site and Dry Fork Station

The Wyoming CarbonSAFE Project is located within the heart of the Powder River Basin (PRB) near Gillette, Wyoming (Figure 1) adjacent to Basin Electric Power Cooperative's Dry Fork Station (DFS) power plant. Dry Fork Station is one of the nation's newest commercial-scale coal-fired power plants and began operation in 2011, and its coal supply is mined locally and provided to the power plant via conveyer belt. The powerplant has an operating lifetime of approximately 80 years, produces a maximum power output of 420 MWatts, and emits roughly 3.3 million metric tonnes (Mt) of CO_2 per annum (Patel, 2018). In addition, the plant received state and DOE funding to build the Wyoming Integrated Test Center which provides the facilities that allow for different carbon capture technologies to be tested on the fairly pure stream of CO_2 that the plant emits after being scrubbed for other pollutants (Patel, 2018; Quillinan and Coddington, 2019).

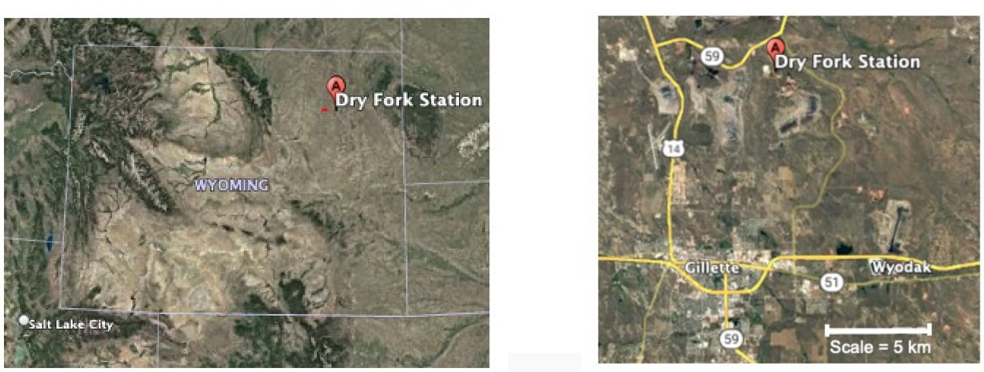

(a) (b)

Figure 1. (a) Google Earth generated aerial photo showing the location of Dry Fork Station within the state of Wyoming. (b) Google Earth generated aerial photo showing the location of Dry Fork Station relative to the city of Gillette, Wyoming.

The initial manifestation of the Wyoming CarbonSAFE project was initiated with Phase I funding from the DOE in 2017. The results of this study proposed an initial injection site located approximately 1 km south of the DFS plant which met all stipulated criteria to move on to a Phase II CarbonSAFE project which commenced in February 2018. Amongst other notable accomplishments, Phase II involved the drilling of a stratigraphic well (PRB #1) to sample and test various target formations in terms of storing $scCO_2$ over the lifetime of the project, as well as the acquisition and processing of a 3D seismic survey (Quillinan et al., 2021). As shown in Figure 2, PRB #1 bottomed out in the Minnelusa Formation, a Permian age collection of dune and shoreline sands (Anna, 2009) with porosities averaging 7% and ranging from nearly zero to as high as 15%. The distinct sand units in this formation are interbedded with dolostones. The top of Minnelusa is about 9335 ft (2845m) below ground surface (bgs), and the sandstones within the upper 150 ft (45m) of this formation serve as the lower unit of the proposed stacked storage interval.

Other units being considered for injection and storage of $scCO_2$ include 96 ft (29m) of sandstones within the Jurassic Hulett formation starting at a depth of at 8274' (2521m), and 76 ft (23m) of sandstones within the Cretaceous Lakota/Fall River Group which is found at approximately 8000 ft (2438m) depth (Quillinan et al., 2021). The Hulett sands encountered in PRB #1 have porosities ranging from 5% to 17% and an average of 11%, while those in the Lakota Formation range from 11% to 14%, with an average of 13%. As shown in Figure 2 this stacked reservoir section is overlain by a thick section of Cretaceous shales that serve as the confining/sealing units to keep the scCO2 from migrating/leaking upward.

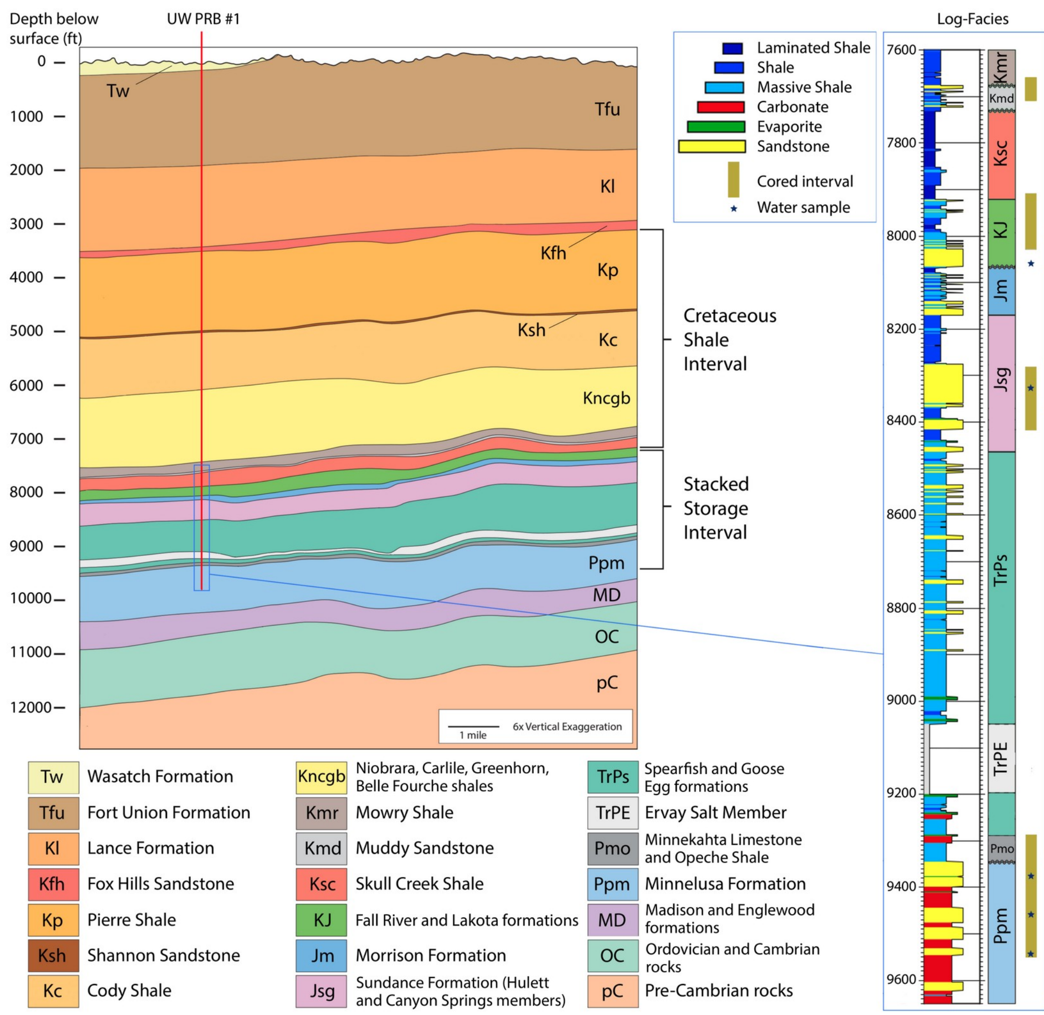

Figure 2. Schematic cross section of the Dry Fork Station area from a 2D seismic line with log-facies interpretation of the primary reservoir units using UW PRB #1 logs on the right. Note the continuity of overlying shale (caprock) layers and the lack of offsetting structure.

Because the results from Phase II showed sufficient storage potential to meet the goals of 50+Mt of CO_2 sequestered over 30 years (Quillinan et al., 2021), the DOE awarded the project a Phase III grant which started in October of 2021 and is to culminate with the submission of a EPA Class VI permit application by the time the project ends in September of 2024. Note that this phase of the project involved the drilling of a second well (PRB #2) approximately 200m to the west of PRB #1, and analysis of log and core data coupled with the results of 3D seismic images show good continuity of the reservoir properties between the two wells in the reservoir units. That said, due to completion problems when running the casing into PRB #1, current plans are to use PRB #1 to inject into the Hullett and Lakota reservoirs, and PRB #2 will inject into the Minnelusa sands (Charles Nye, personnel communication, March 20, 2024).

Electromagnetic Data Acquisition and Assessment

In order to investigate the EM signals generated by DFS as well as other man-made sources, and to determine if EM measurements of high enough quality can be made to sense future sequestered CO_2 at depth, LBNL contracted Zonge International to acquire data in the area surrounding the Dry Fork Station the second half the November, 2022. Below we first provide a schedule and location of the various types of measurements that were made. This is followed by a description and analysis of the data that were collected at two of the measurement locations.

Locations and Timing of CSEM and MT Data Acquisition at the Wyoming CarbonSAFE Site

The Zonge International crew was on site installing transmitters, receivers, and collecting different forms of EM data from November 16 through November 21, 2022. Figure 3 shows an aerial close-up view of the Dry Fork Station site with the locations of the different EM receivers numbered 1 through 11. The map also shows the locations of the transmitters that were employed to collect CSEM data as red lines, while the purple rectangles provide the locations of active coal mines.

At each receiver location, two orthogonal 100m-long dipoles were laid out in North-South and East-West directions to acquire high quality electric field data. The electrodes used for electric field data acquisition consisted of copper-copper sulfate porous pots. The magnetic fields were Zonge ANT/4 induction coil magnetometers. These coils are high-sensitivity magnetic field sensors that are about 3 inches in diameter and 1m long. Like the electric-field antennas, these were laid out orthogonally in North-South and East-West orientations. To reduce wind-generated motion noise the wires for the electric field antennas were covered periodically along the 100m dipole length with piles of surface soil, while the magnetic sensors were buried in shallow trenches that were slightly larger than the coils themselves. The electric and magnetic field data were acquired with Zonge ZEN high-resolution 32-bit receivers.

In terms of the schedule for various measurements, receivers 1 through 5 were installed on the 18th when data acquisition commenced. Note that receivers 1 through 3 were 'permanent' in that once they were installed, they were not moved during the remainder of the survey. Receivers 6 and 7 were deployed on the 19th of November and a full day of data acquired. On the 20th of November, receivers 4 through 7 were picked up and moved to locations 8 through 11, and data were acquired in the afternoon. All receivers were picked up on the 21st that the crew demobilized in the afternoon. Note that much of the spectral data and all of the magnetotelluric (MT) data were acquired over night when conditions are best for MT data acquisition.

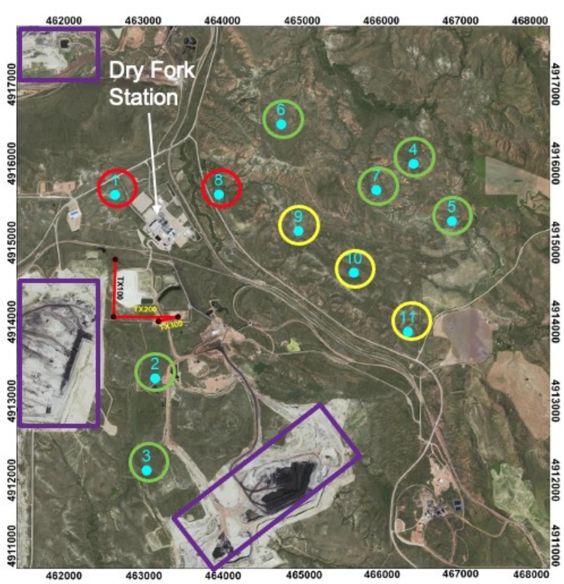

Figure 3. Google Earth generated aerial photo showing the location of the Dry Fork Station power plant relative to the EM receiver sites (numbered blue dots) the CSEM transmitters (red lines) and the active coal mines in the area (purple rectangles). The circles designate the quality of the processed MT data with red designating unusable, yellow probably unusable without additional and time-consuming processing, and green good quality data.

EM Spectral Passive Signal and Background Noise Estimates

As mentioned above, the passive EM data which were used both to estimate background signal and noise as well as for processing to MT impedance estimates were collected overnight. Because of the diffusive nature of EM fields in the earth at MT (and CSEM) frequencies, MT data are processed and analyzed as a function of equally spaced frequencies in the logarithmic rather than linear domain. To avoid the acquisition of larger data sets than are necessary, two different sampling frequencies are used : 4096 Hz to acquire the higher frequency band (from ~1Hz to 1kHz) and 256 Hz to acquire the lower frequency band (0.001 Hz to ~1Hz). The high frequency data were acquired in three-10-minute acquisition periods using a sampling frequency of 4096 Hz, while the low frequency data were acquired in two-6-hour long schedules using a 256 Hz sampling rate. Note that this provides approximately the same number of data samples to process the lower and higher frequency bands, and the break between the high and low frequency bands is instigated in case the EM noise characteristics are changing over time.

For the remainder of this section, we will show data from two or three of the receiver sites shown in Figure 3. Site 1 is the closest to the Dry Fork Station and its proximity to a large electric-power generating facility provides for the highest levels of culturally generated EM noise and thus poorest quality data. Site 10 is further from the station but is located near a major highway and associated train tracks. Site 4 is located the furthest away from both the power station as well as any roads and railways, and thus it provides the best data quality and lowest culturally-generated EM noise levels.

The electric and magnetic field spectra measured at Stations 1 and 4 on November 20 are shown in Figure 4a and 4b, respectively. The yellow and blue curves represent the electric fields while the red and green are the magnetic fields measured at the sites. The upper two plots show the spectra for the 4096 Hz sampling rate, while the two lower plots provide results for the 256 Hz sampling. Note that in each of these there is a vertical blue line at 60 Hz which corresponds to both the largest measured signal as well as the primary frequency of the EM energy generated by the power station. The additional peaks at higher frequencies above this represent the harmonics of 60 Hz. Note because of these large signals at the primary and harmonics, the data above 60Hz is probably unusable at any station in immediate vicinity Dry Fork Station area and can be considered high frequency noise.

Whether or not the data are usable below 60 Hz depends on the component of the field (that is electric or magnetic field) in addition to the distance away from the power station that the receiver is located. Notice that the magnetic fields (red and green curves) exhibit a series of peaks between 4 Hz and 60Hz at Site 1 that are much smaller at Site 4 in terms of the H_x component, and are non-existent in the H_y mode. This is due to the proximity of Site 1 to Dry Fork Station and associated power distribution lines. The Zonge crew noted that the magnetic field sensors were saturating close to the power station, and these spectral peaks are likely due to the clipping of the magnetic field data caused by this phenomenon. Also notice that the electric fields are less noisy than the magnetic fields at low frequencies, especially below 1Hz, and don't exhibit the same peaks. This suggest that for geophysical imaging at the Dry Fork Station and similar locations, reasonable electric field measurements can be made at lower frequencies within 1km of the facility, while the magnetic fields will be unusable at those closer locations.

Magnetotelluric Processing Results

The passive field EM data were processed using a remote reference site as suggested by Gamble et al. (1979) along with the robust processing algorithm implemented by Egbert and Booker (1986). The remote reference technique uses magnetic fields from a station located relatively far away from the site of interest to reduce the effects of correlated noise in the processed MT results. To provide a remote reference sufficiently far away, the Zonge crew installed a 'permanent' site located at WGS84 UTM Zone 13N coordinates of 436158 Easting, 4959801 Northing which is approximately 50km away North-Northwest of Dry Fork Station.

Figure 5 shows processed MT results over a frequency range of 0.001 Hz to 1000 Hz, or periods of 1000 seconds to 0.001 seconds. The top row of each of these plots represents the impedance apparent resistivity, while the bottom shows the impedance phase. Note that the dark blue curves represent the XY mode of the impedance which from a simplistic view point is calculated by dividing the North-South component of the electric field by the East-West magnetic fields, while the red curves represent the YX mode which uses opposite components compared to the XY mode. The first thing to note is that the Site 1 results are very erratic and noisy over the entire frequency range both in apparent resistivity and phase. This is indicative of noisy conditions and these processed MT results are essentially unusable. Site 10 which was designated as 'marginal' is also very noisy, especially at the higher frequencies. However, the lower frequency data look of usable quality and thus this site might be usable with appropriate data editing. Site 4 on the other hand displays very smooth curves from one frequency to the next which is what MT data should look like. There are a few noise spikes above 60Hz and at the lowest frequencies as well as around 0.1 Hz, but in general most of these data are usable. In addition, at the higher frequencies the apparent resistivities lie between 5 and 10 Ωm, and then decrease to around 2 Ωm at about 0.1Hz. A visual analysis of the induction log collected in well PRB1 indicates that these are reasonable values with the near surface down to around 1130m depth showing log apparent resistivities between 5 and 10 Ωm, while below 1130m and down to 1900m the resistivity drops to around 2Ωm in the log. A more robust assessment of the accuracy and quality of the MT soundings is provided in the modelling section below.

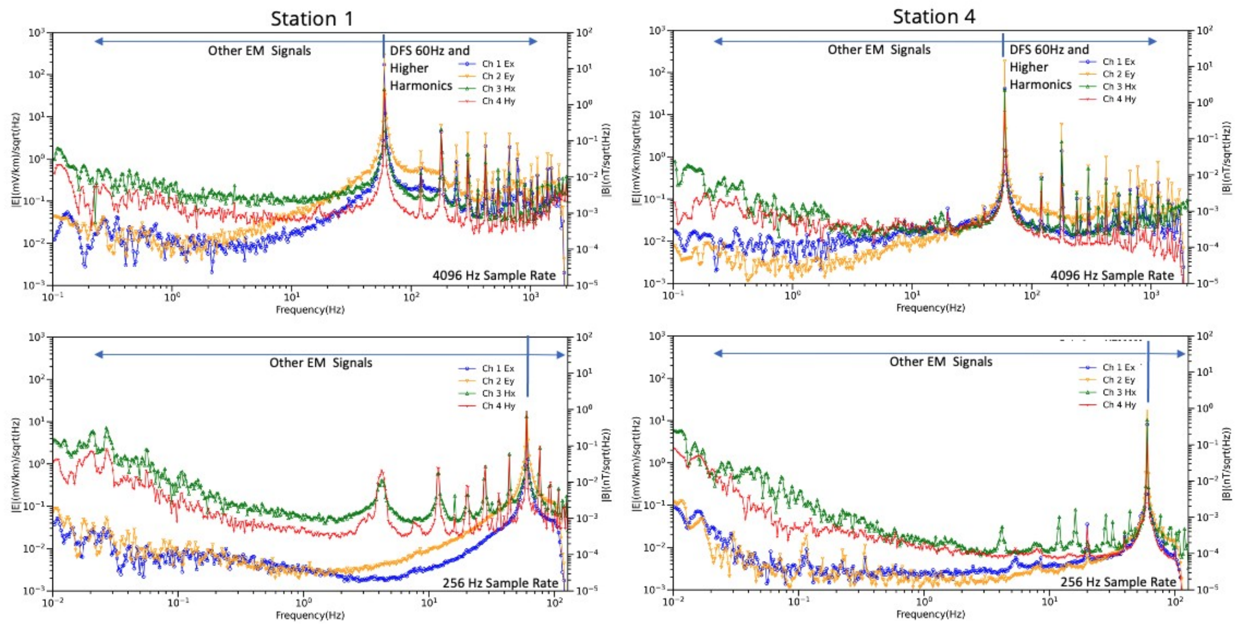

Figure 4. Passive electromagnetic signals measured on November 20 at Sites 1 (left) and 4 (right) during the Dry Fork Station survey. The upper plots are the spectra resulting from the 4096 Hz data acquisition, while the lower plots represent the 256 Hz sampled spectra. The blue and yellow curves represent the electric fields measured in the North-South and East-West directions, respectively, while the green and red curves represent the magnetic fields measured at the sites in the same respective directions. The scale on the left side of the figure is for the electric fields, and on the right side the magnetic field scale is displayed.

The quality of the processed MT data has been classified on the survey map (Figure 3) using color coding. The two red sites that are closest to the powerplant produce unusable data (red circles) while the sites along a main road and rail line (yellow circles, i.e., sites 9, 10 and 11) are also likely unusable due to motion noise caused by traffic and trains. The MT data collected at the sites designated with green circles have quality similar to Site 4 in Figure 3 and thus should be completely usable. Note that the MT data will likely not be sensitive to the injected CO_2 at depth, but rather could be used to monitor changes in groundwater quality as well as to make sure receivers are functioning properly.

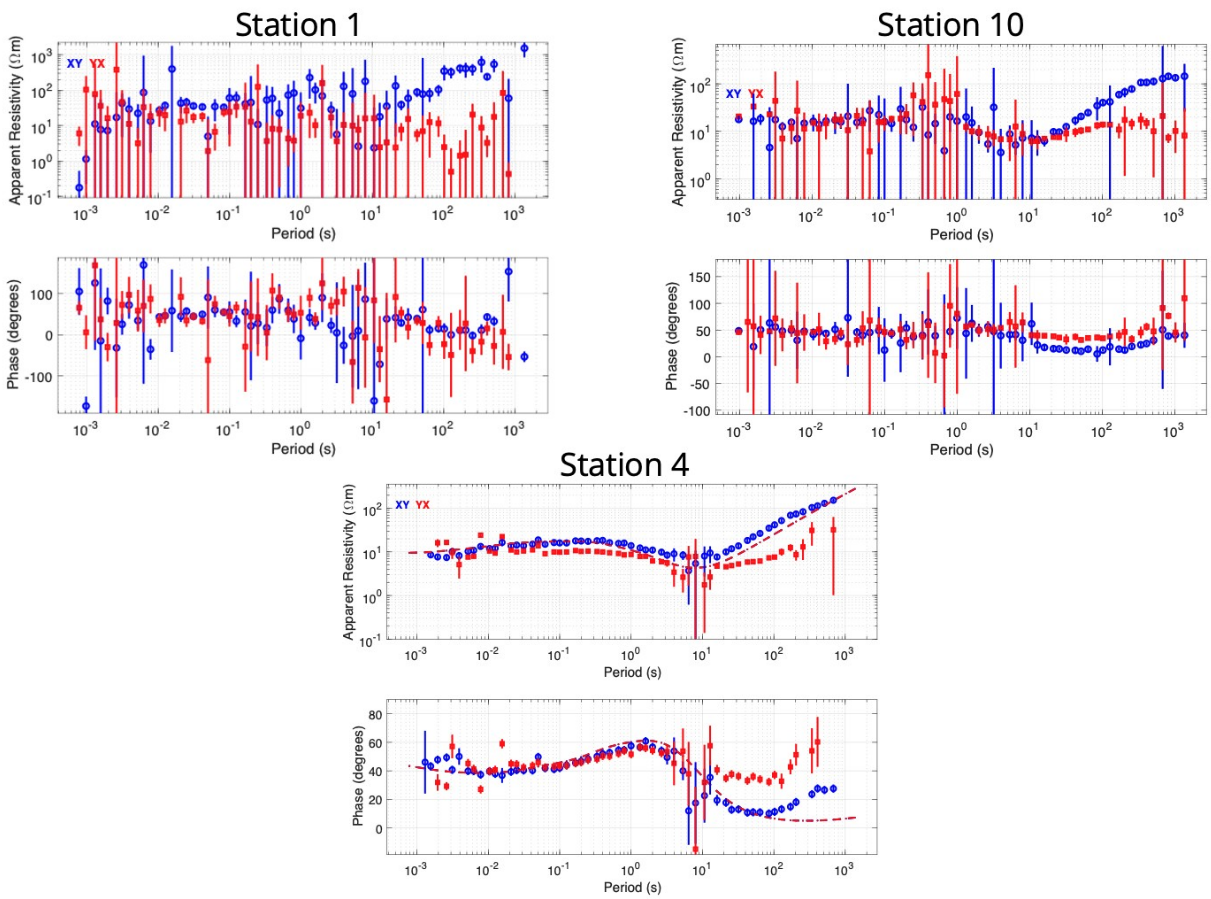

Figure 5. Processed MT results at Sites 1, 10 and 4 for EM data collected over night on November 20, 21, and 20, 2022, respectively. The dark blue curve represents the XY mode impedance data where the electric fields are aligned North-South and magnetic fields East-West, while the red shows the YX mode where the fields are aligned in the opposite manner. The upper plots are of impedance apparent resistivity, while the bottom plots are of impedance phase. The dotted red line represents the forward calculation of the 1D model constructed from well logs and shown in Figure 8 below.

CSEM Data Acquisition and Processing Results

The locations and layout of the three electric sources are shown in Figure 3, and at a larger scale in Figure 6 below. The electrical contact on the surface at both ends of TX100 were made by pounding twenty aluminum stakes into the ground and connecting them with electric fence wire. The western electrode for TX200 was the same as the southern electrode for TX100, while the eastern side of the source was grounded by connecting the transmitter wire to a flange on the PRB #1 well via a jumper cable. For TX300 both ends of the source wire were connected to PRB #1 and PRB #2 using this same procedure.

The CSEM data were recorded using a transmitter current that consisted of a 0.125 Hz square waveform. This results in a frequency domain response at the primary frequency as well as odd harmonics. The resulting data were processed by stacking each single waveform to produce a stacked and rectified single waveform to reduce noise, normalizing the resulting stacked waveform data points by the transmitter current, and then Fourier transforming the data from the time domain to the frequency to produce usable frequency domain data starting at 0.125Hz, and as mentioned extending upward at odd harmonics (e.g. 0.375 Hz, 0.625Hz, 0.875 Hz, 1.125Hz, ….). After transformation to the frequency domain, the magnetic field data had an additional step applied where by each frequency was multiplied by a magnetic-sensor specific calibration coefficient to convert the measured data from coil-output-voltage to magnetic field. The power of transmitted signals in each of the harmonics falls off at a rate approximately equivalent to 1/ frequency therefore there is less signal present at higher frequencies compared to lower frequencies. Note that CSEM data were acquired at the active receiver sites each day while each transmitter was active for approximately a one-hour time period.

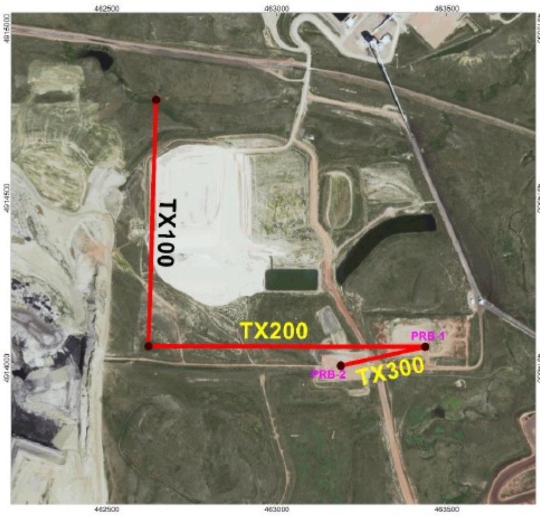

Figure 6. Enlarged view of the CSEM source locations used in the Wyoming CarbonSAFE EM measurement campaign.

Figure 7a shows the spectrum of the data at Sites 1 and 4 collected while TX200 was transmitting, and Figure 7b while TX300 was active. These have been plotted in the same format as that used for the passive EM spectral plots in Figure 4. We have not included measurements when TX100 was operating due to 1) the resulting spectral amplitudes look very similar to that produced when TX200 was operating, and 2) the numerical modeling exercise below indicated that there is no sensitivity to the injected scCO_2 when the source is not connected to the steel well casing of the injection wells. Above 60 Hz Figures 4 and 7 look similar due to the signal that is being generated by Dry Fork Station. However, the two sets of figures look different below 60 Hz, especially in the band from 0.125 Hz to 10 Hz as the 'spikes' that occur in this band in Figure 7 represent the signals produced by the transmitters.

The signal levels at the base frequency and odd harmonics are much larger in magnitude than the signals in between the spikes. These lower magnitude signals in between the spikes are the natural EM background energy as well as that generated by the power station and can be considered the CSEM measurement noise floor. The fact that the transmitter signature is much larger than the background and power-station generated signals suggests that if these type of EM measurements are sensitive to the electrically resistive CO_2 replacing brine in the injection zone, the CSEM method should be applicable to monitoring conformance for sequestration at the Wyoming CarbonSAFE site. Note that when TX200 is transmitting the signal-to-noise-ratio (SNR) for the electric fields at the base frequency at Site 1 is around 80dB while at Site 4 it is approximately 46dB. It is much larger at Site 1 due to the closer proximity of the site to the source. When TX300 is operating the electric field SNR's at sites 1 and 4 drop to approximately 60dB and 40 dB respectively. This reduction in amplitude is due to the fact that length of the wire on the surface for TX300 is shorter than that of TX200 which implies a smaller transmitter 'moment', or power. Also note that the magnetic fields tend to have poorer SNR's than the electric fields.

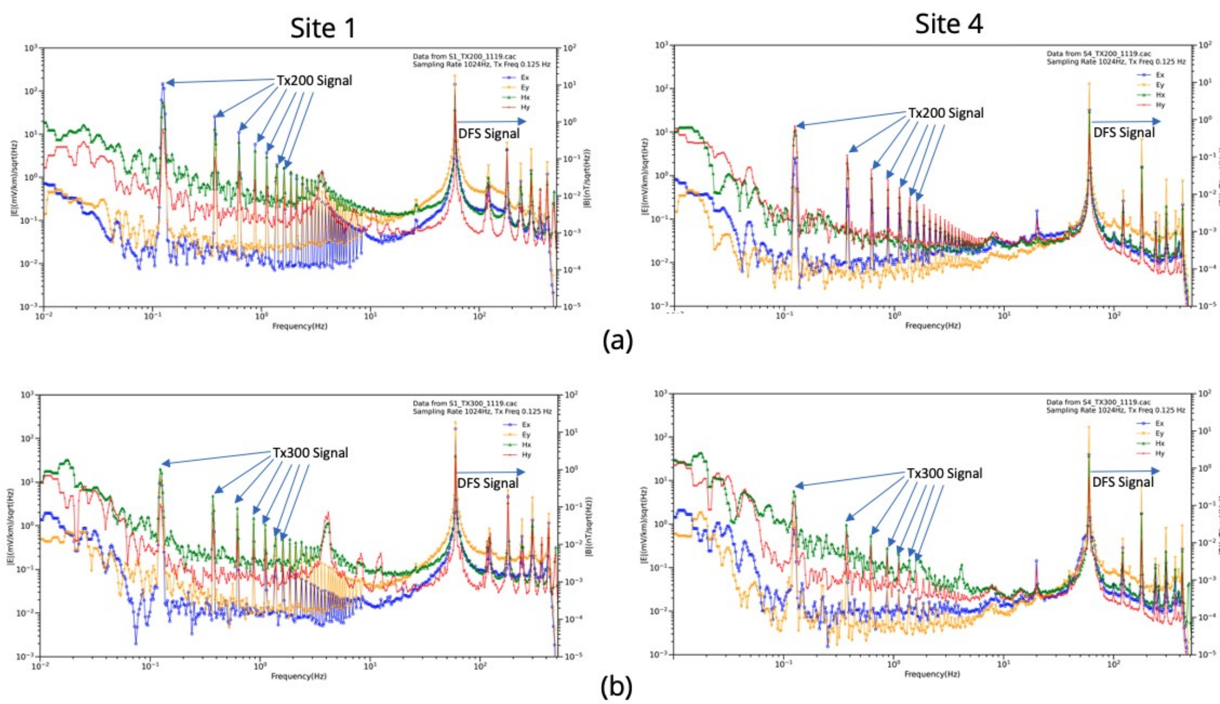

Figure 7. Electromagnetic signals measured at Sites 1 (left) and 4 (right) during the Dry Fork Station survey while (a) TX200 and (b) TX300 were transmitting. The blue and yellow curves represent the electric fields measured in the North-South and East-West directions, respectively, while the green and red curves represent the magnetic fields

measured at the sites in the same respective directions. The ‘spikes’ from 0.125 through 10 Hz represent the TX200 and TX300 measured signals at the receivers. The scale on the left side of the figure is for the electric fields, and on the right side the magnetic field scale is displayed.

Numerical Sensitivity Studies

In order to determine if various EM methods will be able to provide sensitivity to the injected plume, we first built a 3D resistivity model that captures the true background structure based on induction logs collected in the PRB#1 well. Next, we generated a series of hypothetical resistivity models with representations of the CO_2 injection scenarios, and then ran a series of numerical simulations to produce synthetic MT and CSEM data that would be measured on the surface of the earth prior to and after plume injection using various configurations of grounded electrical sources where by injection well casings are connected to a 0.25Hz source. The simulated results are then compared to the measured data from the survey to ascertain the sensitivity of this type of CSEM survey to the plume at depth. Below we first provide more details of the construction of resistivity models, and then follow this with an analysis of the resulting MT and CSEM simulations.

Creation of the resistivity models

The resistivity models were constructed using the following steps.

- The induction log from PRB#1 were analyzed visually, and average resistivities assigned to depth intervals ranging from 5m to several hundred meters thick (Figure 8). Note that the thicker zones represent depth intervals where the resistivity is somewhat consistent compared to a visually determined average value and/or is well above the proposed injection intervals. Because the well log does not extend all the way to the surface nor into the basement, resistivities at the top and bottom as well as the depth to basement are rough estimates. The layering becomes finer around the five proposed injection zones as provided by staff members of the Wyoming CarbonSAFE project. The resulting resistivity model is provided in Figure 8 both in table and graphical format.

- The second step involved assigning porosities to the five proposed injection zones. These were estimated using neutron porosity logs collected in well PRB#1 with the estimated values shown in the left column of Table 1.

- Next, Archie's Law (Archie,1942) was used to estimate resistivities in the five injection zones assuming a CO_2 saturation of 60%. Archie's law is given as

$$R_t = a R_w \varnothing^m S_w^{-n} \quad (1)$$

where R_t is the true bulk-rock resistivity, R_w the resistivity of the water filling the pore space, ϕ is the porosity, and S_w is the water saturation. Note that the injected supercritical CO_2 is assumed to be of very high resistivity and thus is not included in the expression. The constants a, m, and n are empirical constants and were assumed to have values of 1,2, and 2, respectively, which were found to be 'average' values for sandstones by Archie (1942). The resulting calculated resistivities for the five injections zones are provided in Table 1. As a side note, we currently do not have specific information on the typical range of CO_2 saturation when injecting CO_2 into sandstone at the Wyoming CarbonSAFE site. However, we anticipate that 60% represents the upper end of CO_2 saturation that we might expect. Therefore, the modeling results presented here reflect a best-case scenario.

- For numerical purposes the next step was to upscale the zones within and between the planned thin injection zones into thicker reservoir injection units; a 90m thick zone extending from 2455 to 2545 m depth to represent the planned injection in PRB#1, and a 60m thick zone extending from 2850 m to 2910 m which covers the planned injection intervals in PRB#2. This upscaling is necessary to prevent the inclusion of thin, elongated cells within the numerical model which makes the finite element solution of Um, et al (2020) numerically unstable. Also, to better account for the current flow within the alternating conductive and resistive layers for the models that include the thin layers of injected CO_2, the resistivities within these zones were calculated anisotropically with the geometric mean of the layer resistivity used to determine the vertical resistivity, and the harmonic mean the horizontal. This produces injection zones as shown in Figure 9 that are less resistive in the horizontal direction than in the vertical which will produce current flow patterns similar to that of alternating conductors and resistors. Using these upscaled resistivity values, two different plume models were created as shown in Figure 9. An 'early' plume representing a relatively short time after injection has begun, and a 'late' plume representing something akin to 20 years of injection. Note that the latter value was provided by reservoir modeling results conducted by others involved in the project. Note that injection A is the upscaled injection zones planned for PRB#1, and B that corresponding to injection through PRB#2.

- The last step for the creation of the numerical model was to accurately simulate the sources that were deployed during the data acquisition experiments as shown in Figure 9. The choice to connect to the casings of wells PRB1 and PRB2 are due to previous work that shows that this provides a pathway for more current to get down to the reservoir level than provided by surface electrodes alone (eg. Marsala et al., 2014, MacLennan et al., 2016). Note that because TX100 involved only surface electrodes and did not connect to one of the well heads, we decided only to simulate TX200 and TX300. In addition, not only did we simulate connecting to the top of the well casing which was the case in the field, but we also simulated placing the electrodes at the bottom of the wells to enhance sensitivity to the target zone (Marsala et al., 2014). Note that in order to simulate energized well casings for 3D geology/structures we employed the workflow outlined in Um et al. (2024) which simulate the steel casing in a layered medium, calculates the current density versus depth on the outside of the casing, and then replaces the energized casing with an equivalent line of dipoles whose amplitude and phase vary with depth to match the currents. This allows us to simulate the response when both well PRB#1 and PRB#2 are energized simultaneously without having to discretize the casing finely in order to handle the high conductivity contrast between casing and the surrounding formation.

Layered Resistivity Model

Depth Range (m)	Resistivity
0-50	10 Ωm
50-490	20 Ωm
490-1110	10 Ωm
1110-1520	2 Ωm
1520-2050	4 Ωm
2050-2355	3 Ωm
2355-2415	2 Ωm
2415-2455	10 Ωm
2455-2460	3 Ωm **
2460-2490	8 Ωm
2490-2520	3 Ωm
2520-2540	7 Ωm
2540-2545	2 Ωm**
2545-2770	10 Ωm
2770-2805	1 Ωm
2805-2850	10 Ωm
2850-2865	3 Ωm**
2865-2885	20 Ωm
2885-2890	4 Ωm**
2890-2905	15 Ωm
2905-2910	6 Ωm**
2910-3600	20 Ωm
3600-inf	1000 Ωm

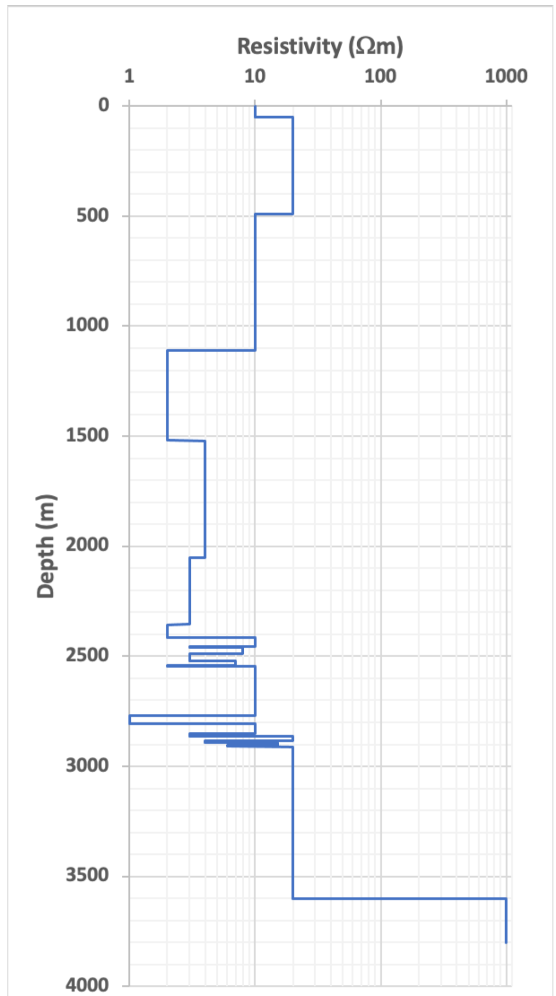

Figure 8. The one-dimensional resistivity model constructed by visually averaging induction log data collected in the PRB1 well at the Wyoming CarbonSAFE site. The table on the left details the averaged resistivity and layer thicknesses used, with the ** representing the proposed injection depths provided by members of the Wyoming CarbonSAFE project. The right side shows the model in graphical form in terms of resistivity versus depth.

	Porosity	Reservoir Resistivity (S_W=1)	Fluid Resistivity	Reservoir Resistivity (S_W=0.4,S_{CO2}=0.6)
Reservoir 1	0.35	3 Ωm	0.61 Ωm	30.93 Ωm
Reservoir 2	0.30	2 Ωm	0.42 Ωm	24.46 Ωm
Reservoir 3	0.20	3 Ωm	0.35 Ωm	54.13 Ωm
Reservoir 4	0.15	4 Ωm	0.30 Ωm	83.33 Ωm
Reservoir 5	0.10	6 Ωm	0.24 Ωm	153.09 Ωm

Table 1. Computed resistivities in the five planned injections zones at the Wyoming CarbonSAFE site using Archie's law (Archie, 1942) and assuming 60% CO_2 saturation during/after injection.

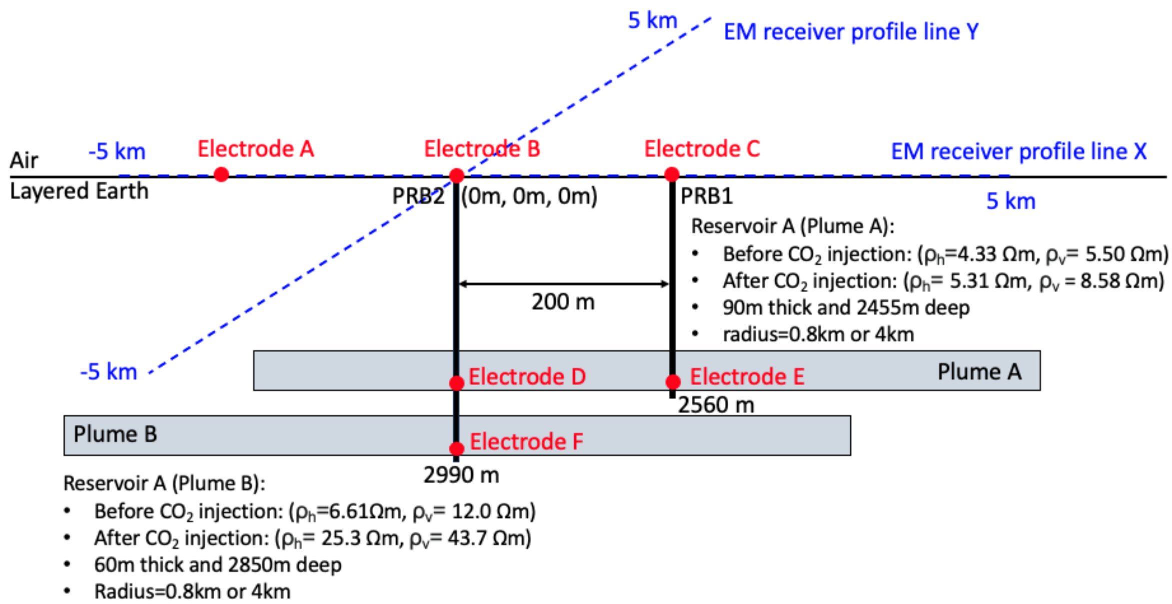

Figure 9. Cross-section through the 3D resistivity models used for the Wyoming CarbonSAFE modeling. The background layered resistivity model outside of the injection zones is described by the thicker layers in Figure 8. The thinner layers within injection zones as shown in Figure 8 have been upscaled assuming anisotropic averaging to Plumes A and B as shown here. The electrodes A through F were arranged to simulate variations of the real sources TX200 and TX300 that were employed in the field. When comparing the model to the Google Earth Photos in Figures 3 and 6, Line X corresponds to the East-West direction and Line Y North-South.

Numerical Simulation of the MT Data

The first step in the numerical simulation was to simulate the 1D MT response to the layered model shown in Figure 8. Although the MT method is well known to not be sensitive to thin resistors at depth (Constable and Weiss, 2006) such as that produced by the injection of $scCO_2$ into deep saline reservoirs, running the 1D calculation and comparing to the measured MT data does provide checks on both the quality of the MT data collected at the site as well as the realism of the 1D background model constructed from the well log. The results of this process are shown for Site 4 as the dashed red line in the right-hand side of Figure 5. Note that the comparison between the numerical results and XY mode is excellent from the high frequencies down to 100 seconds at which point the numerical solution diverges from the measured data. These results not only suggest that the upscaled well log is providing a good representation of the sedimentary section above the basement at the site, but also that the geology of the site is fairly 1D as deviations between the 1D model and measured data only occurs when the data are sensing well into the basement and/or laterally away from the site.

Numerical modeling of CSEM Sensitivity

The CSEM fields were next computed using the finite element code of Um et al. (2020) for a variety of different sources involving energized steel casing(s) with the different connection points for the sources shown in Figure 9. Note that during the casing modeling to determine the equivalent distribution of electric dipoles, we assumed a uniform steel casing with an electrical resistivity of 10^{-6} Ωm and a relative magnetic permeability of 100. For this set of calculations we employed a frequency of 0.25 Hz which was determined optimal in terms of signal strength and at the same time provided numerical stability with the 3D modeling codes used.

In terms of the locations of the receivers and components of the fields that were computed, receivers were placed along two lines (Profile lines X and Y) as shown in Figure 9 at 200m intervals from -5km to 5km. Five components of the electromagnetic fields, the X and Y components of electric field, and X, Y, and Z components of the magnetic field, were computed at each location. In general, none of the magnetic fields showed a response due to the CO_2 and thus plots of magnetic fields are not included here. In terms of the electric fields, the Y component along Line X is 'null coupled' to the X directed transmitters, and thus this component along that line was zero and thus not plotted below. In addition, the X component of the field measured along the Y line showed little sensitivity to the plumes. Therefore, what is included below are plots of the X component of the electric field along the X line, and the Y component of the electric fields along the Y line.

Note that for efficiency in the modeling study, results for the larger plume radii of 4km were computed first for all electrode combinations shown in Figure 9. These showed that only two of the sources provided for a change in amplitude that was 5% or above, which would be considered substantial enough to be measured: a source with electrodes at points A and F, and a source composed of electrodes at the bottom of both wells (points E and F). Because only these two sources showed a response for the larger plume, these were the only two sources for which the modeling study was completed for the smaller (0.8km) plume and that are included in the sensitivity analysis below. However, in order to compare the field results to the numerical analysis in terms of SNR of the measurements, we first present electric field modeling examples that mimic source configurations that were used in the field. Thus, in Figure 10a we present fields calculated at 0.25 Hz for a source connecting to electrode positions A and C in Figure 9, while in in Figure 10b we provide results for a source connecting points B and C, that is, at the top of the well heads.

When comparing the result in Figure 10 to those in Figure 7, the first thing that is noticeable is the difference in scale with Figure 7 having much larger amplitudes than those in Figure 10. This is due to two factors, the first being that the units in Figure 7 are in mV/km while in Figure 10 the units output by our numerical codes are in V/m. Thus, this produces a discrepancy of 6 orders of magnitude. In addition, the numerical results in Figure 10 are computed for a source current of 1 Ampere while the results in Figure 7 were measured using a source current between 17 and 20 Amps and the fields were not normalized by this value. Note that the Zonge transmitter is a 'constant voltage' device, and thus the variation in current output is a product of the applied voltage and the overall contact resistance of the source. The higher the antenna contact resistance, the lower the applied current. In any event, if one were to multiply the results in Figure 10 by 1.7×10^7 to 2.0×10^7 you can see that the amplitudes will be very similar.

None of the results in Figure 10 show any sensitivity to the plumes. That is the amplitude curves for the different scenarios all overlie each other. Also notice that the E_x fields in each case are about 1 order of magnitude larger than the E_y fields, at least at the far offsets.

In terms of configurations that do indicate sensitivity to the plume, Figures 11 and 12 show the electric field amplitudes and phase results for the source that connects locations A and F in Figure 9, while Figures 13 and 14 show the same type of plots for the source that connects points E and F. Each one of these figures shows one component at 0.25 Hz along a line, with the first set of Figures showing E_x along Line X, and the second E_y along Line Y. The top set of three plots in each figure are from left to right the amplitude, the phase, and the percent difference in amplitude for the smaller (0.8km) radius plumes, while the bottom set of plots are for the larger (4km) radius plumes. Each one of these plots shows the response due to each the two plumes separately, as well as combined. One thing to note is that the amplitudes in these plots are very close to those shown in Figure 10, and thus we don't see a loss in signal strength due to the electrodes being located at the bottom of the well. However, because a longer wire will be required to locate the electrodes at the bottom of the wells, the amount of current that can be injected into the subsurface will lessen due to the increased resistance provided by the additional wire.

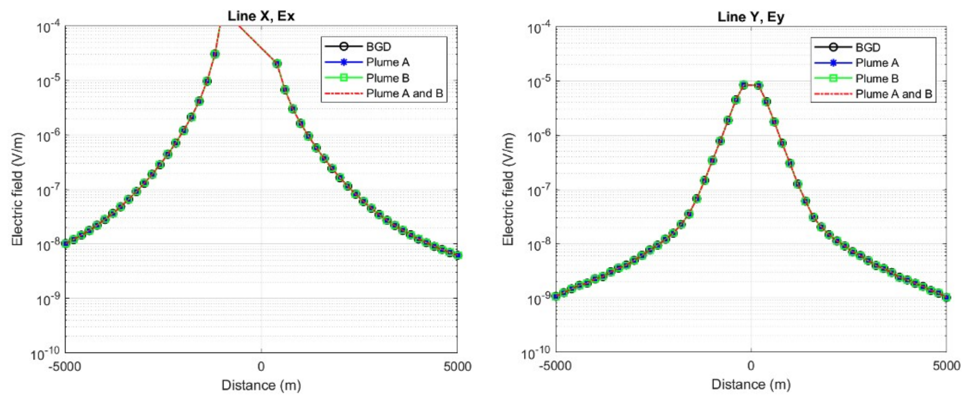

(a)

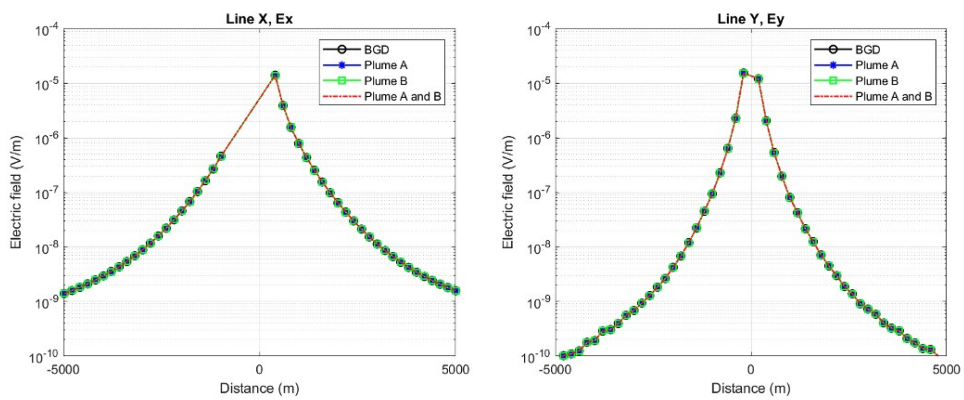

(b)

Figure 10. (a) E_x electric field amplitude along line X (left) and E_y electric field amplitude along line Y (right) at 0.25Hz for the source connecting points A and C in Figure 9. (b) E_x electric field amplitude along line X (left) and E_y electric field amplitude along line Y (right) at 0.25Hz for the source connecting points B and C in Figure 9. Plume A denotes the upper plume surrounding PRB1 in Figure 9, and Plume B denotes the lower plume surrounding PRB2.

An analysis of these figures shows that the best sensitivity along these two receiver lines occurs along the Y line when measuring the E_y component. For the source connecting points A and E, the maximum response is about 5% in amplitude for the small plumes and 5.5% to 6.5% for the larger plumes. For the source connecting the bottom of both borehole the responses jump to 50% to 75% amplitude. E_x along the X line shows some sensitivity, but generally it is much less than the response on the Y line perpendicular to the source polarization.

Further analysis of the plots indicate another interesting fact in that the response from Plume A (the upper plume surrounding PRB1) is always much smaller than the response from Plume B (the lower plume surrounding PRB2). Analysis of Figure 9 strongly suggest this is due to the much smaller resistivity change due to CO_2 injection in Plume A than Plume B that is the result of the upscaling of Plume A only involving two thin (5m) injections zone, whereas Plume A has three injection intervals, one of which is 15m thick. A last interesting note in the analysis is that the sensitivity when both plumes are present is often smaller than when just Plume B is present. This suggests that there is some type of ‘interference’ occurring between the individual EM responses when both plumes are present.

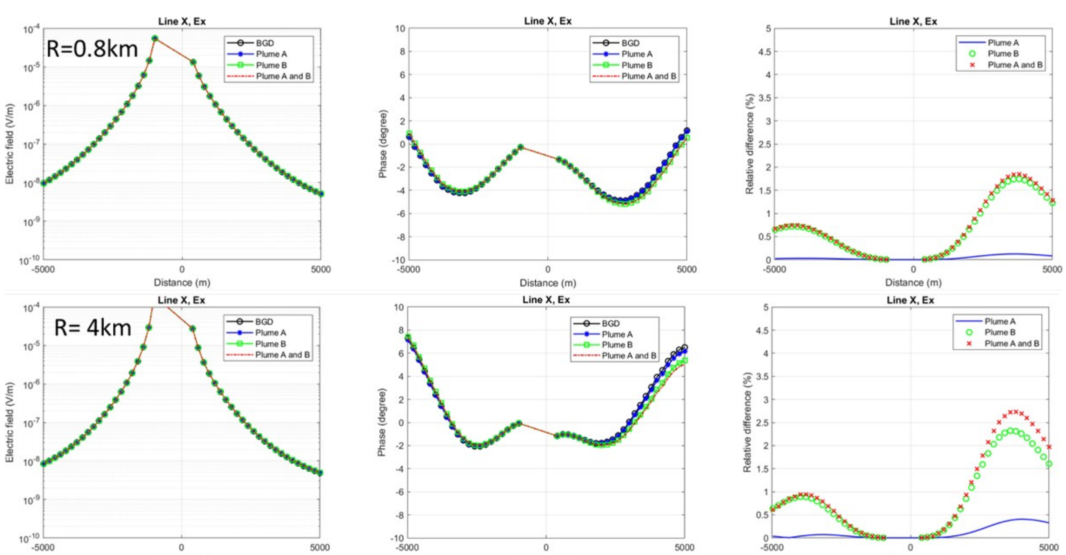

Figure 11. E_x component of electric field at 0.25Hz computed along Line X in Figure 9 for the source connecting points A and F. The top line is for the smaller 0.8km radius plumes, while the bottom is for the larger 4km radius plumes. Plume A denotes the upper plume surrounding PRB1 in Figure 9, and Plume B denotes the lower plume surrounding PRB2.

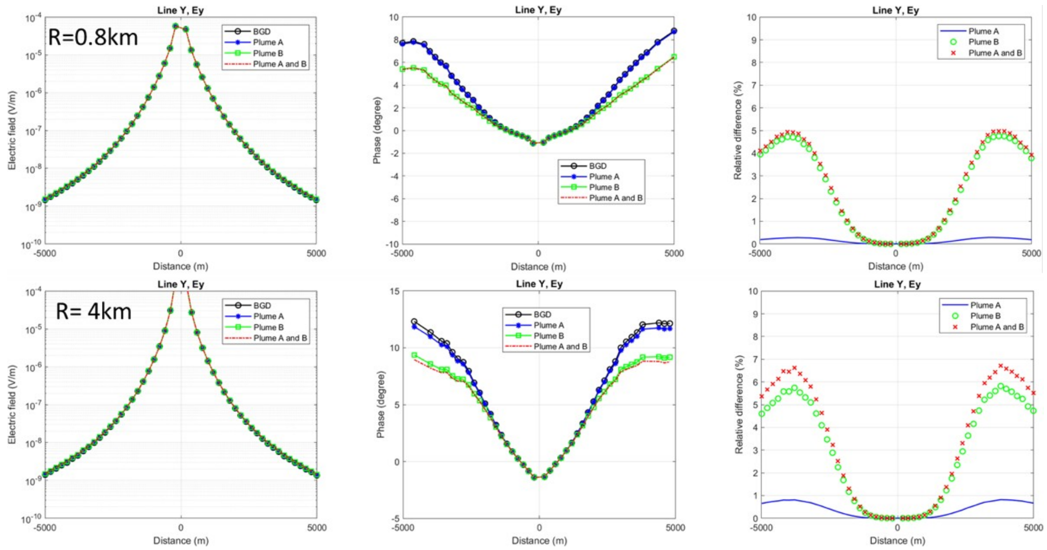

Figure 12. E_y component of electric field at 0.25Hz computed along line Y in Figure 9 for the source connecting points A and F. The top line is for the smaller 0.8km radius plumes, while the bottom is for the larger 4km radius plumes. Plume A denotes the upper plume surrounding PRB1 in Figure 9, and Plume B denotes the lower plume surrounding PRB2.

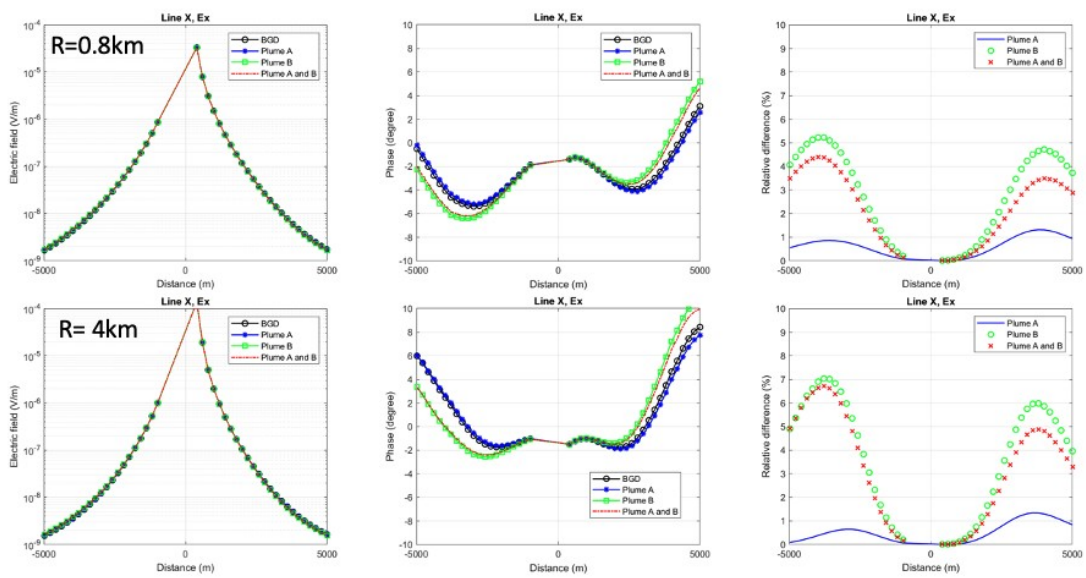

Figure 13. E_x component of electric field at 0.25Hz computed along line X in Figure 9 for the source connecting points E and F. The top line is for the smaller 0.8km radius plumes, while the bottom is for the larger 4km radius plumes. Plume A denotes the upper plume surrounding PRB1in Figure 9, and Plume B denotes the lower plume surrounding PRB2.

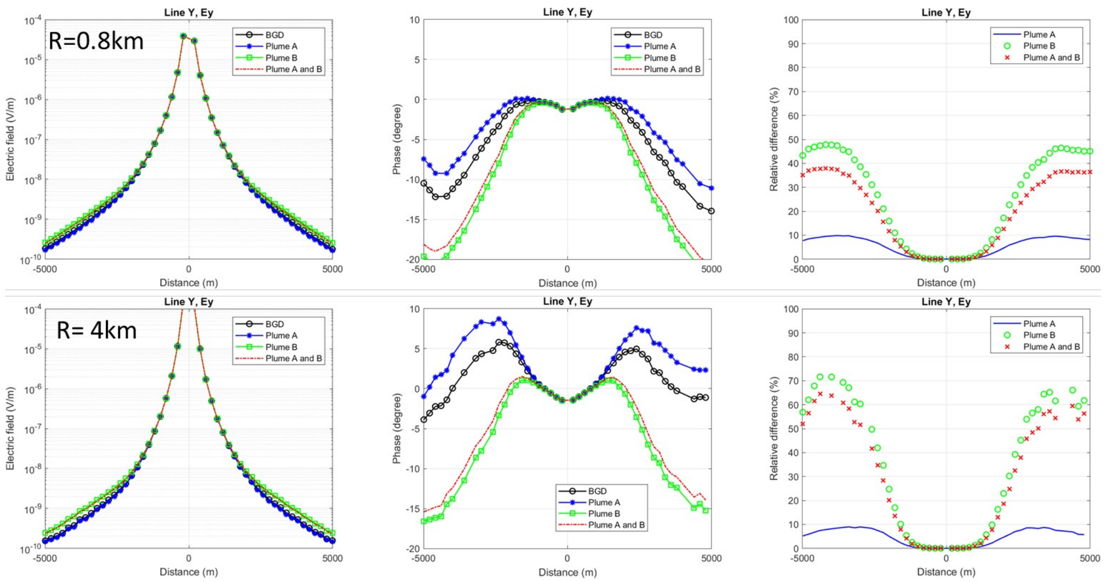

Figure 14. E_y component of electric field at 0.25Hz computed along line Y in Figure 9 for the source connecting points E and F. The top line is for the smaller 0.8km radius plumes, while the bottom is for the larger 4km radius plumes. Plume A denotes the upper plume surrounding PRB1 in Figure 9, and Plume B denotes the lower plume surrounding PRB2.

The last step in the analysis is to compare the amplitudes of the signals shown in the plots above to actual noise levels measured at site. First, comparing analysis of Sites 1 and 4 in Figures 4 and 7 along with a unit conversion to be in accordance to the electric field units of V/m employed in Figures 10 though 14 indicate a noise level at 0.25 Hz of around 5×10^{-10} V/m during the day when the CSEM data were collected, and slightly better overnight when the passive data were acquired. Note that this is noise level is well below the amplitude for most of the configurations in Figures 10 through 14. The exception to this is for the E_y fields measured along the Y line when the two well heads are connected (Figure 14). However even in this case the signal is above the noise at distances away from the source where significant anomalies are produced. In addition, both sites show good signal-to-noise ratios of at least 40dB's at the primary transmission frequency of 0.125Hz. Combining this analysis with the simulated signal levels shown suggests that as long as the connection electrodes can be placed in the bottom of the wells, that the proposed CO_2 injection at the Wyoming CarbonSAFE site should be able to be monitored using EM methods.

Conclusions and Discussion:

To evaluate the EM geophysical methods for monitoring CO_2 sequestration efforts at the Wyoming CarbonSAFE project that is adjacent to the Dry Fork Station coal fired power plant, LBNL contracted Zonge International to collect passive and controlled source EM data in November of 2022. Both electric and magnetic fields were collected at 11 different locations. Measurements were made at positions from less than 1km away from the power plant out to 4km away. The passive data were not only used to provide spectral EM noise measurements that are generated by electricity production, but also showed that useful MT data can be collected as long as the site is located more than 2km away from the power plant as well as active roads and rail lines.

CSEM data were collected using three different source configurations: one running in a North-South configuration using surface electrodes separated, an East-West dipole that just over 800m long that used the steel well casing of PRB#1 as the eastern most electrode, and a third source that was approximately 200m long and connected the two wells at the site (PRB#1 in the East and PRB#2 to the West). The CSEM data were collected using a square wave with a base frequency of 0.125HZ. Comparing the EM noise measurements to the CSEM data show measurable electric and magnetic field signals at all sites that are well above noise signals produced by the power plant.

The last step in the process was to conduct a 3D numerical modeling study to mimic the geometry of the measurements made at the Wyoming CarbonSAFE site, as well as explore other potential source and receiver configurations that will provide optimal sensitivity to the proposed injected plumes. The models completed to date show that there exists measurable signal out to 4 to 5km away from the wells and there is sensitivity to the injected CO_2 if the wells are included as part of the EM source and the connection electrodes are placed at the bottom of the injection wells.

The fact that sensitivity exists only when electrodes are placed at the bottom of the wells does pose some problems in terms of the practicality of the measurements. One solution is to bring a wireline logging truck out to the site each time monitoring measurements are to be made as was reported by MacLennan (2022) and Marsala et al. (2014). However, this poses an issue with cost if we are to use injection wells as that will require injection to be shut down, production tubing to be pulled, pressure management equipment to be installed, etc. In-zone monitoring wells could also be used but similar issues will exist with that in using these boreholes as if the injection zone is over-pressured, pressure management will need to be deployed while the tool is in the well. Since the CCUS business is a tax-incentive driven business model, any additional costs associated with monitoring surveys cuts into profits (see Alumbaugh et al.(2024) for a brief description of commodity versus tax-incentive markets).

To cut monitoring costs, permanent installations may be required. Completing the well with the connection cable on the outside of the casing may be an option as wells with fiber optical sensing often run the protected fiber on the outside of the casing, but this adds complication to the completion process and some operators fear that imperfect cement jobs around the cable/fiber could lead to leakage pathways. Another option is to strap the wire to the production tubing and then make contact to the inside of the well with a metallic centralizer. This method has yet to be tested but may provide an avenue in the future to lower the costs of this type of monitoring.

Acknowledgement

We thank J. Fred McLaughlin, Charles Nye, and Robert Gregory of the University of Wyoming for their help in gaining access to the Dry Fork Station site and surrounding mine lands, and for providing information regarding CCUS plans for the site. This research was supported by U. S. Department of Energy, National Energy Technology Laboratory, CCSMR program, under the U.S. DOE Contract No. DE-AC02-05CH11231.

References:

Alumbaugh, D. L., Correa, J., Jordan, P., Petras, B., Chundur, S., & Abriel, W. (2024). An assessment of the role of geophysics in future US geologic carbon storage projects. The Leading Edge, 43(2), 72-83.

Anna, L.O., Klett,T.R., and Le, P.A., 2009, Total petroleum systems and geologic assessment of oil and gas resources in the Powder River Basin Province, Wyoming and Montana; U.S. Geological Survey Digital Data Series DDS–69–U.

Colombo, D. and Rovetta, D., 2018. Coupling strategies in multiparameter geophysical joint inversion. Geophysical Journal International, 215(2), pp.1171-1184.

Constable, S. and Weiss, C. J., 2006, Mapping thin resistors and hydrocarbons with marine EM methods: Insights from 1D modeling; Geophysics, **71**(2), G43-G51.

Egbert, G. D., and Booker, J. R., 1986, Robust estimation of geomagnetic transfer functions; geophysical Journal International, **87**(1), 173-194.

Gallardo, L.A. and Meju, M.A., 2003. Characterization of heterogeneous near-surface materials by joint 2D inversion of dc resistivity and seismic data. Geophysical Research Letters, 30(13).

Gamble T. D. Goubau W. M. Clarke J., 1979. Magnetotellurics with a remote reference, Geophysics, 44,53–68.

Giraud, J., Pakyuz-Charrier, E., Jessell, M., Lindsay, M., Martin, R. and Ogarko, V., 2017. Uncertainty reduction through geologically conditioned petrophysical constraints in joint inversion. Geophysics, 82(6), pp.ID19-ID34.

MacLennan, K., 2022, Monitoring CO2 storage using well-casing source electromagnetics: The Leading Edge, **41**, no. 2, 107–113, https://doi.org/10.1190/tle41020107.1.

Marsala, A.F., Hibbs, A.D., and Morrison, H.F., 2014, Borehole casing sources for electromagnetic imaging of deep formations. Paper presented at the SPE Annual Technical Conference and Exhibition, Amsterdam, The Netherlands, https://doi.org/10.2118/170845-MS.

Patel, S., 2018, Dry Fork: a model of modern U.S. Coal Power; Power Magazine, https://www.powermag.com/dry-fork-a-model-of-modern-u-s-coal-power/.

Quillinan, S., McLaughlin, J. F., and Coddington, K., Commercial-scale Carbon Storage Complex Feasibility Study at Dry Fork Station, Wyoming; United States: N. p., 2021. Web. doi:10.2172/1780712.

Quillinan, S., and Coddington, K.,2019, Integrated Commercial Carbon Capture and Storage (CCS) Prefeasibility Study at Dry Fork Station, Wyoming; United States: N. p., Web. doi:10.2172/1557442.

Um, E., D. Alumbaugh, M. Wilt, E. Nichols, Y. Li, S. Kang and K. Osato, 2023, 3D Numerical Modeling Analysis of Deep Borehole Electromagnetic Measurements with Energized Casing Source for Fracture Mapping at the Utah FORGE Geothermal Site, submitted to Geophysical Prospecting for review.

Um, E.S., Kim, J. and Wilt, M., 2020. 3D borehole-to-surface and surface electromagnetic modeling and inversion in the presence of steel infrastructure. *Geophysics*, *85*(5), pp.E139-E152.

Vasco, D., T. Daley and A. Bakulin, 2014, Utilizing the onset of time-lapse changes: a robust basis for reservoir monitoring and characterization, Geophysical Journal International, 197, 542–556.

Wilt, M. J., and Alumbaugh, D. L., 1998, Electromagnetic methods for development and production: state of the art: *The Leading Edge*, **17**, 487-490.